Rydberg electromagnetically induced transparency of ^{85}Rb vapor in a cell with Ne buffer gas

Nithiwadee Thaicharoen [*]
Department of Physics and Materials Science, Faculty of Science, Chiang Mai University, Chiang Mai 50200, Thailand

Ryan Cardman and Georg Raithel [†]
Department of Physics, University of Michigan, Ann Arbor, Michigan 48109, USA

(Received 17 August 2023; revised 11 March 2024; accepted 3 May 2024; published 4 June 2024)

Motivated by an interest in measuring electric fields in low-pressure noble-gas discharge plasmas and in dusty plasmas via noninvasive Stark-effect spectroscopy, we investigate Rydberg electromagnetically induced transparency (EIT) of ^{85}Rb atomic vapor in a glass cell that contains a 5-Torr neon buffer gas. We find that at low probe power the Ne buffer gas induces a positive frequency shift of the Rydberg-EIT lines of about 70 MHz as well as a broadening of about 120 MHz, with minimal dependence on the principal quantum number of the Rydberg states. The EIT line shift predominantly is a sum of a positive term from *s*-wave scattering between the Rydberg electron and the Ne atoms, and a negative term from the polarization of the Ne atoms within the Rydberg atom. The polarization shift is lesser in magnitude, resulting in the observed net positive shift. The line broadening is largely due to the Ne polarization. Our experimental results are in good qualitative agreement with our theoretical model, in which the shift is linear in buffer-gas density. Our results suggest that Rydberg EIT is suitable for noninvasive measurement of electric fields in buffer-gas cells that sustain a plasma discharge, and that it can serve as a direct spectroscopic probe for buffer-gas density at low pressure.

DOI: 10.1103/PhysRevApplied.21.064004

I. INTRODUCTION

Electromagnetically induced transparency (EIT) involving Rydberg-atom spectroscopy in room-temperature atomic vapors has become an important technique for electric field sensing, offering sensitivity in metrology applications [1–3] as well as avenues towards nontraditional radio receivers [4–6]. Rydberg Stark spectroscopy and direct-particle detection was used to measure macroscopic and microscopic electric fields in ion plasmas prepared from laser-cooled atom clouds [7,8]. In laser-generated plasmas in thermal atomic vapors, Rydberg-EIT Stark spectroscopy was employed for noninvasive all-optical electric field measurement [9,10]. Also dc electric fields of charges released by photoillumination of a borosilicate vapor cell were analyzed using Rydberg-EIT spectroscopy of Rb nD_J Rydberg levels [11]. These developments suggest that Rydberg EIT may have the potential to serve as a noninvasive plasma electric field probe in glass tubes, vacuum systems, or vapor cells that harbor a low-pressure discharge or an inductively coupled plasma.

As a step towards noninvasive, spatially resolved Rydberg-EIT field sensing in discharge plasma and dusty plasma, it is necessary to assess the viability of Rydberg EIT of a suitable atomic sensor species, such as rubidium or cesium, under the presence of an inert gas that sustains the plasma discharge. Setting a buffer-gas pressure limit for Rydberg EIT is an important step in staking out the applicability range of Rydberg EIT for plasma field diagnostics, because the result will limit the types of plasmas for which the method will work. The determination of such a buffer-gas pressure limit necessitates a study of the effects of buffer gas on Rydberg-EIT spectra.

Previous work [12] has explored the effects of Rb–Ne collisions on $5S_{1/2} \rightarrow 5P_{3/2} \rightarrow 5D_{5/2}$ EIT linewidths in a buffer-gas cell. In our present work, we observe ^{85}Rb Rydberg EIT at principal quantum numbers of $n \sim 40$ in a cell with a 5-Torr neon buffer gas. We measure the frequency shift and line broadening of the EIT signal due to the background gas. At high probe-laser power, we observe a transition from EIT to electromagnetically induced absorption (EIA). The observed features do not significantly depend on n. Earlier Rydberg-atom spectroscopy in buffer gas [13–16] did not involve a near-resonant intermediate atomic state. Our work demonstrates that Rydberg EIT, a contemporary noninvasive spectroscopic method that

[*]Corresponding author: nithi@umich.edu
[†]Corresponding author: graithel@umich.edu

does require a near-resonant intermediate state, is viable in buffer gas with pressures up to at least 5 Torr. Our results on Rydberg level shifts and broadening are similar to those in the earlier works. The buffer-gas effect on the Rb D_2 line and on the intermediate state of the ladder-type Rydberg-EIT system is seen to be considerably less important than the effect on the Rydberg state. Our study presents a stepping stone towards employing Rydberg-EIT spectroscopy of Stark shifts as a noninvasive, spatially resolved probe for electric fields in plasmas with pressures up to about 5 Torr.

Our work may find applications in the diagnostics of rf or dc rubidium plasma lamps [17,18], which are commonly used as spectroscopic frequency references and for optical pumping of alkali vapors in magnetic-field-sensing cells. Moreover, plasma often contains charged dust particles [19]. Such dusty plasmas appear, for instance, in astrophysical settings (including the B ring of Saturn [20], Martian dust devils [21], and the moon [22]), as well as in technical plasmas (including fusion [23] and microfabrication devices [24]). The dynamics of such plasmas are being explored in ground-based [25,26] and microgravity setups [27] using low-pressure noble-gas plasmas, which are seeded with dust particles. Rydberg EIT could be ideal for nonintrusive measurement of electric fields, Debye shielding and particle interactions [28], and electric field wakes [29] in a dusty plasma. Furthermore, alkali-metal vapors mixed with a low-pressure inert buffer gas could possibly serve as a common platform for Rydberg-EIT electric field sensors and other sensors, such as Faraday [30] and spin-exchange relaxation free [31] magnetometers.

II. RYDBERG ATOMS IN A BUFFER GAS

Atoms in highly excited Rydberg states exhibit sensitivity to their environment. The interaction between Rydberg atoms and ground-state atoms, here referred to as perturbers, which may be of the same or a different atomic species, gives rise to Rydberg-level shifts and broadening. The shift can be attributed to two main effects [32–34]. The dominant effect arises from the scattering of the Rydberg electron by the perturbers within a Rydberg-atom volume of $\sim \frac{4}{3}\pi(2n^2a_0)^3$, with Bohr radius a_0. This scattering effect can be explained by a Fermi interaction [35], and the resulting angular frequency shift in units of rad/s is given by

$$\Delta\omega_{\rm sc} = 2\pi a_s \left[\frac{e^2 a_0}{4\pi\epsilon_0\hbar}\right] N, \tag{1}$$

where $\hbar$ is the reduced Planck's constant, e is the elementary charge, ϵ_0 is the permittivity of the vacuum in F/m, a_s is the low-energy s-wave scattering length in meters, and N is the volume density of the buffer-gas atoms. Higher partial waves tend to be unimportant because of the low kinetic energy of the Rydberg electron, which is small in comparison with p-wave and higher centrifugal energies near the buffer-gas atoms.

The second effect originates from the interaction between the ion core of the Rydberg atom and the perturbers. When a Rydberg atom is immersed in a medium containing ground-state atoms or molecules, the atomic electric field induces a polarization in the perturbers, which in turn gives rise to an electric field that shifts the Rydberg levels. The resultant polarization-induced frequency shift can be obtained from the impact approximation [32,33], and is given by (in units of rad/s)

$$\Delta\omega_{\rm p} = -6.21\left[\frac{\alpha e^2}{\hbar(4\pi\epsilon_0)^2}\right]^{2/3} v^{1/3}N, \tag{2}$$

where α represents the polarizability of the perturber in $\mathrm{C\,m^2/V}$, and v is the mean relative velocity between the Rydberg atoms and the perturbers in m/s. The total energy shift experienced by the Rydberg atom is the sum of both effects, $\Delta\omega_{\rm total} = \Delta\omega_{\rm sc} + \Delta\omega_{\rm p}$.

In addition to frequency shifts, polarization and electron scattering can also lead to level decays, denoted $\gamma_{\rm p}$ and $\gamma_{\rm sc}$, respectively. It was found that the level decay mainly comes from the polarization of the perturbing atoms [33], i.e., $\gamma_{\rm p} >> \gamma_{\rm sc}$, and that the decay rate

$$\gamma_{\rm p} = 2\times 3.59\left[\frac{\alpha e^2}{\hbar(4\pi\epsilon_0)^2}\right]^{2/3} v^{1/3}N. \tag{3}$$

The value of $\gamma_{\rm p}$ is equivalent with a full width at half maximum (FWHM) line broadening in units of rad/s.

Through two-photon, Doppler-free spectroscopy, the broadening and shifts of Rb nS and nD Rydberg levels in the presence of inert perturbers has been experimentally observed in [13] for He, Ar, Ne, Kr, and Xe, in [14] for He, Ar, and Xe, in [15] for He and Ar, and in [16] for Ne, Kr, and H_2. For these experiments, the effects of buffer-gas pressure broadening by the intermediate $5P_{1/2}$ and $5P_{3/2}$ levels could be ignored because they were very far off-resonance. This is, however, not the case in our work. Pressure broadening of the Rb D_2 line due to binary interactions with noble gases has been observed in [36] for pressures of up to 1.1 kTorr. Recently, ultra-high pressures of He and Ar on the order of 10^5 Torr interacting with a Rb vapor were spectroscopically studied in [37]. In the present work, the Ne pressure is 5 Torr, which leads to a D_2 line broadening on the order of $\gamma_{D_2} \sim 2\pi \times 50$ MHz [38]. This is consistent with the fact that Doppler-free saturated absorption spectra of the buffer-gas cell show no significant remnant features of the $5P_{3/2}$ hyperfine structure, which have separations in the range of 50 to 100 MHz. Since we observe Rydberg-EIT linewidths that are considerably larger, at the level of precision of our current study we neglect the

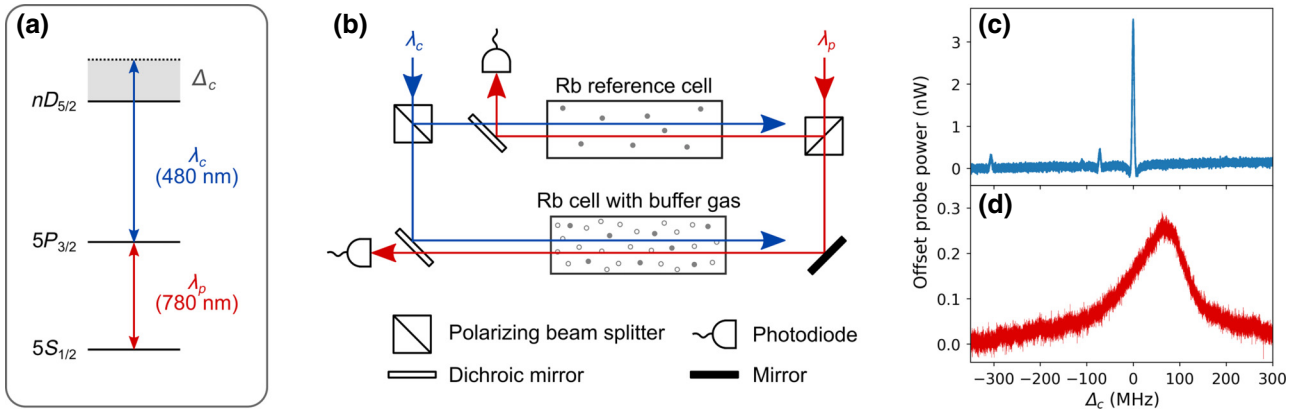

FIG. 1. (a) Rubidium energy levels used in this work. The probe laser (λ_p) is on-resonance with the $5S_{1/2} \leftrightarrow 5P_{3/2}$ transition, while the coupling laser (λ_c) is detuned from the $5P_{3/2} \leftrightarrow nD_{5/2}$ transition by Δ_c. (b) Illustration of the Rydberg-EIT setup (lenses are omitted for simplicity). The EIT signals are detected simultaneously from both the Rb reference cell and the Rb cell with buffer gas. The 34D EIT signals from the Rb reference cell and the Rb cell with buffer gas are shown in (c) and (d), where the probe powers are 170 nW and 130 nW, respectively, and the coupling-beam powers are approximately 2 mW and 35 mW.

effect of γ_{D_2} on the Rydberg-EIT linewidth. As such, based on $\gamma_p >> \gamma_{sc}$ and $\gamma_p > \gamma_{D_2}$, we compare our measured Rydberg-EIT linewidths only with estimates for γ_p.

While we were unable in our experiment to change the buffer-gas pressure, it is noted that the observables in Eqs. (1)–(3) all scale linearly in N (and hence in pressure, at fixed temperature). We further note their independence from the principal quantum number n. While the quantities described by Eqs. (2) and (3) are unrelated to n, for Eq. (1) the n independence largely follows from a picture in which the scattering shift scales with the number of buffer-gas atoms within the Rydberg atom times the Rydberg electron's wave-function density. Since the Rydberg-atom volume is $\sim \frac{4}{3}\pi(2n^2a_0)^3$, as mentioned earlier in this section, the number of buffer-gas atoms within the Rydberg atom scales as n^6. Over the range $34 \leq n \leq 46$ investigated in our work, at 5 Torr the number of buffer-gas atoms within the Rydberg atoms varies from about 1000 to 7000. These are large numbers with $\lesssim$3% statistical variation in time. The $\propto n^6$ dependence of the perturber atom number is accompanied by a change in wave-function density, which scales as n^{-6}. The two changes cancel in the resultant shift. This is in accordance with Eq. (1), which is n independent and proportional to the number of buffer-gas atoms per volume, N.

III. EXPERIMENTAL SETUP

We perform the EIT experiment using ^{85}Rb atoms with the relevant energy levels shown in Fig. 1(a). The probe laser with a wavelength of $\lambda_p = 780$ nm is close to resonance with the $F = 3$ to $F' = 4$ hyperfine component of the $5S_{1/2} \leftrightarrow 5P_{3/2}$ transition. The EIT signal is measured as a function of the coupling-laser frequency (wavelength $\lambda_c \approx 480$ nm), which is scanned over the $5P_{3/2} \leftrightarrow nD_{5/2}$ transition. The coupling-beam detuning is denoted by Δ_c.

We simultaneously extract EIT signals from two EIT beam lines, as shown in Fig. 1(b). The upper beam line, which serves to produce a reference spectrum, utilizes a buffer-gas-free Rb vapor cell. The reference EIT signal allows us to calibrate the frequency axis for Δ_c, as well as to mark the coupling-laser frequency of the shift-free EIT line. In the lower (signal) beam line, the EIT signal is acquired using a cell that contains Rb vapor and a Ne buffer gas of nominally 5-Torr pressure. The probe and coupling lasers are split between the reference and signal beam lines using polarizing beam-splitter cubes, and are then counter-propagated through the respective cells. In each cell, both beams have parallel linear polarizations. After passage through the cells, probe and coupling beams are separated using dichroic optics. The reference and signal probe beams are simultaneously detected using a pair of identical silicon photodiodes and low-noise transimpedance amplifiers (TIAs), and the respective data traces are recorded. We perform 100 scans per data set, and present averages over the 100 scans.

The Rb vapor cell in the reference (upper) beam line in Fig. 1(b) is 7.5 cm long and held at room temperature (291 K). The probe and coupling beams in the reference line are approximately Gaussian and have $1/e^2$ drop-off radii of the intensity distribution of $w_0 = 300$ and 500 μm, respectively. The cell that contains the buffer gas, located in the signal line, is 5 cm long and heated to 303 K, so that both the reference and the buffer-gas cell have a peak absorption of about 70% on the $5S_{1/2}$, $F = 3 \leftrightarrow 5P_{3/2}$ transition. The probe and coupling beams in the signal (lower) line have Gaussian beam parameters of $w_0 \approx 150$ μm.

The reference EIT signal is shown in Fig. 1(c). The strongest EIT peak is from the $5S_{1/2}, F = 3 \leftrightarrow 5P_{3/2}, F' = 4 \leftrightarrow 34D_{5/2}$ cascade, which has the largest electric dipole moment among the allowed intermediate-state hyperfine levels (quantum number F'), and is the least diminished

by optical pumping into the uncoupled $5S_{1/2}$, $F = 2$ level. The two small peaks that bracket the $-$ 100 MHz mark are from the intermediate-state levels $5P_{3/2}$, $F' = 3$ and $F' = 2$. These are small in size mostly due to optical pumping during the atom-field interaction time, which is a few microseconds in the buffer-gas-free cell. Interaction-time broadening is irrelevant in both reference and buffer-gas cells. All observed frequency splittings between the $5P_{3/2}$ hyperfine peaks carry a Doppler scaling factor of $(\lambda_p/\lambda_c - 1) = 0.63$. The leftmost peak in Fig. 1(c) is attributed to the $5S_{1/2}$, $F = 3 \leftrightarrow 5P_{3/2}$, $F' = 4 \leftrightarrow 34D_{3/2}$ cascade. Noting that the Doppler scaling factor for Rydberg lines is unity, the splitting between the largest $34D_{5/2}$ peak and the $34D_{3/2}$ peak in Fig. 1(c) equals the $34D_J$ fine-structure splitting, which is 306.061 MHz (based upon published quantum defects [39]). This splitting is used for calibration of the frequency axis of the reference and signal spectra, which are simultaneously acquired.

A typical Rydberg-EIT signal at a low probe intensity, obtained from the cell with buffer gas, is shown in Fig. 1(d). The EIT signal from that cell has an asymmetric shape, and in the case shown the peak is shifted positively from the reference EIT line by 68 ± 1 MHz. In the following we study the dependence of shift and linewidth on principal quantum number n. We will then explore effects observed at high probe intensity.

IV. FREQUENCY SHIFTS AND LINEWIDTHS

To study the effect of the buffer gas on the EIT signals for a range of different Rydberg states, we take Rydberg-EIT data over an n range of 34 to 46. The data are evaluated by analyzing the peak shift and the FWHM of the EIT line. We extract the relative frequency of the EIT peak in the signal beam, which equals the frequency shift of the EIT caused by the buffer gas. The frequency-shift results are shown in Fig. 2(a) for probe powers of 0.06, 0.13, and 0.22 μW, corresponding to the probe Rabi frequencies listed. The observed EIT-line frequency shifts are in the range of 60–73 MHz and average to about 67 MHz, with the low-power data clustering around 70 MHz.

To arrive at an estimate for the actual Rydberg-level shift, we apply a small correction caused by the buffer-gas-induced shift of the intermediate EIT state $5P_{3/2}$. At our pressure, the D_2 line is expected to shift by approximately -10 MHz [38]. Due to applicable Doppler factors in our EIT setup [40], only about 60%, or about -6 MHz, contribute to the observed EIT line shift. The experimental Rydberg-level shifts are thus expected to be about 6 MHz higher than the EIT line shifts observed in Fig. 2(a), leading to an average Rydberg-level shift of about 73 MHz and a shift range of 66–79 MHz. This result agrees well with the observations in [16], where the shift rate was measured to be 12 ± 1 MHz/Torr for high n (which would lead to a shift of 60 ± 5 MHz for 5 Torr of Ne buffer gas). Further, the shift decreases by up to about 10 MHz when the probe power increases, and it appears overall to decrease by a few megahertz when n increases. The weak n dependence agrees with a semiclassical calculation in [41], which shows that the frequency shift of the Rydberg nD state slightly decreases as n increases.

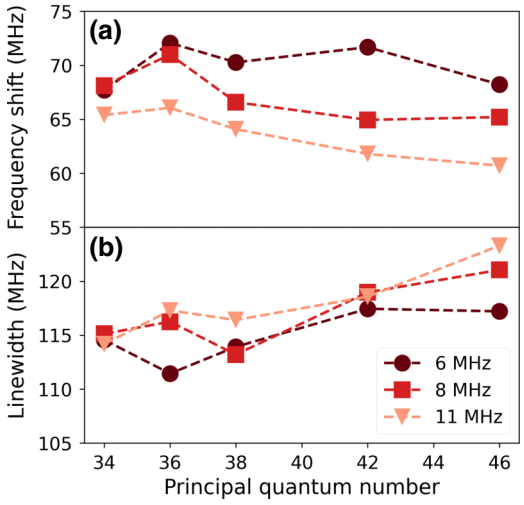

FIG. 2. (a) Frequency shift of the EIT signal from the Rb cell with buffer gas relative to the $nD_{5/2}$ peak for $F' = 4$ in the reference EIT spectrum versus n, at several probe powers with estimated Rabi frequencies at the beam center shown in the legend. The plot data are extracted from local parabolic fits to the peaks in spectra. Fit error bars are smaller than the marker size. (b) Corresponding FWHM of the EIT peaks. The FWHM values are obtained from the roots of the first derivatives of smoothed EIT curves [see Figs. 1(d) and 3]. Statistical uncertainties are smaller than the marker size.

For a quantitative comparison with theory, we first calculate the electron-scattering shifts using Eq. (1). For the low-energy s-wave scattering length, a_s, several of the previously computed values include, from low to high, $a_s = 0.2a_0$ [42], $0.227a_0$ [43], and $0.24a_0$ [33]. A table listing both theoretical and experimental values for a_s is provided in [44]. Over the range $0.2a_0 < a_s < 0.24a_0$, $\Delta\omega_{sc}/(2\pi)$ varies from 195 MHz to 234 MHz. The shift from the Ne polarization due to the Rydberg atom, obtained from Eq. (2) and using $\alpha = 2.66$ in atomic units [33], is $\Delta\omega_p/(2\pi) = -122$ MHz. The net Rydberg-level shift from these two effects, $\Delta\omega_{total}/(2\pi)$, then ranges between 73 MHz and 112 MHz. It is seen that the shift from the calculation has the same sign in theory and experiment, confirming that the low-energy s-wave scattering length a_s is positive (which is not the case for some other buffer gases) and that the scattering shift is dominant. Furthermore, depending on what exact value for a_s is adopted, the calculated net shift is about 0% to 50% larger than the average experimental value of ≈ 73 MHz from the previous paragraph. Hence, we claim good qualitative agreement.

To discuss these findings, we first note that the overall spread of data previously reported for a_s has the largest

effect on the spread of our calculated Rydberg-level shift, $\Delta\omega_{\text{total}}$. Our experimental result is in accordance with the lower end of previously reported a_s values, $a_s \approx 0.2a_0$. As to additional effects that might matter, we note that the Rydberg-EIT line may be slightly pulled to lower frequencies by the weak EIT peaks that are visible in Fig. 1(c) but that are hidden in Fig. 1(d). Furthermore, the Ne buffer-gas pressure of 5 Torr has an uncertainty of 5% according to manufacturer information. Along the same line, one may speculate that differences in cell temperature during cell fabrication and the cell's eventual operating temperature could in principle cause a mild buffer-gas density drop.

Further progress in comparing experimental buffer-gas-induced Rydberg-EIT shifts and theoretical estimates would require a refinement of theoretical models for a_s as well as a full density-matrix model for Rydberg EIT that covers the effects of the buffer gas on all involved atomic levels. In experimental work, one may consider a determination of the absolute Ne density with an independent, quantitative method. These research directions are, however, outside the scope of our present work.

We next extract the FWHM of the EIT signal from the cell with buffer gas for several probe powers and n values. As shown in Fig. 2(b), the observed FWHM of the EIT signal from the cell with the buffer gas is between 110 and 125 MHz, which greatly exceeds the width of the reference EIT lines. The FWHM of the buffer-gas EIT slightly increases with an increase in n, but it is not significantly dependent on the probe power. This agrees well with the calculation in [41], which shows that, for Rydberg nD states, the FWHM of the Rydberg line should slightly increase with n. A calculation of the broadening γ_{p} from the polarization effect [Eq. (3)] yields a FWHM of 144 MHz, which is $\approx 20\%$ larger than the experimentally observed width. We note that the effects that we neglect here may contribute to the experimentally observed line broadening, including broadening from the weak EIT peaks that are visible in Fig. 1(c) but that are hidden in Fig. 1(d), as well as the line broadening γ_{D_2} [which is small compared to γ_{p} but still substantially > 0 (see Sec. II)]. The results on the EIT linewidth could also indicate that the exact density of Ne atoms in the cell is slightly lower than the density at 5 Torr and at room temperature.

V. EFFECTS OF PROBE POWER

Finally, we study the effects of probe power on the Rydberg-EIT signal obtained from the cell with buffer gas by varying the probe power from $P_p = 0.06$ to 1.79 μW. The central probe-laser electric field is $E_p = \sqrt{2I_p/(c\epsilon_0)}$, with central intensity $I_p = 2P_p/(\pi w_0^2)$ and $w_0 \approx 150$ μm for the signal beam line. The probe Rabi frequency $\Omega_p/(2\pi) = \mu_{12}E_p/h$, where $\mu_{12} = 1.892\, e\, a_0$ [45] is the probe-transition dipole moment. The EIT signals from the $34D_{5/2}$ state are shown in Fig. 3 for five values of the probe

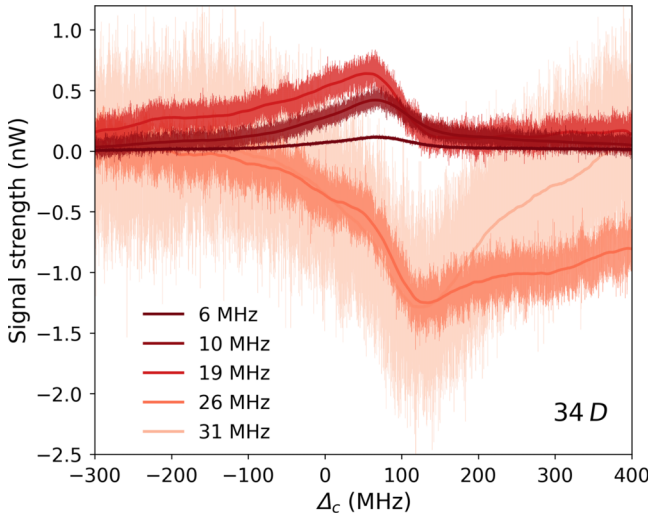

FIG. 3. EIT signals of Rb $34D_{5/2}$ Rydberg atoms in the cell with buffer gas for probe-laser powers ranging from 0.06 to 1.79 μW. The colors of the plots correspond to probe-laser Rabi frequency, $\Omega_p/(2\pi)$, indicated in the legend. To allow for a comparison of the signals on a fixed scale for the transmitted probe power, the plots are vertically shifted so that they level out at zero at large detunings. Also, the TIA gain is decreased with increasing probe power to avoid saturation. The plot shows data at the full TIA bandwidth as well as smoothed curves that allow for an easier comparison of the atomic response across the full probe-power range.

Rabi frequency. The noise increase at high probe power is attributed to an increase in shot noise as well as an increase in TIA bandwidth at lower gain. Over the gain values used, the bandwidth of the TIA (model SRS SR570) increases from 200 Hz to 2 kHz with increasing probe power. Hence, the signals at higher probe powers have considerably larger noise on the utilized absolute-power scale. In Fig. 3, we include smoothed curves that allow for an easier comparison of the signal behavior over the entire probe-power range.

It can be seen in Fig. 3 that at low probe powers (Rabi frequency $\lesssim 10$ MHz, as used in Sec. IV) the EIT lineshape is approximately invariant, and that at low probe powers both the EIT line height and area increase with probe power. In the limit of vanishing probe power a linear behavior is expected. Also, the shape of the EIT signal is asymmetric, with a longer tail on the negative side. We speculate that this behavior may come in part from the blending of intermediate-state hyperfine structure, which adds to the nD-line broadening [36]. For probe Rabi frequencies between 6 and 19 MHz, the EIT peak shifts slightly from about 67 MHz to 55 MHz, while the shape and width of the peak still largely remain the same. At probe Rabi frequencies exceeding ~ 20 MHz, the signals invert in shape and turn into EIA, with the center of the EIA dip located ~ 50 MHz above the low-power EIT peak. The transition from EIT to EIA at high power may be due

to factors such as optical pumping, diffusive interaction-time lengthening, and velocity-changing collisions. The theoretical explanation of this consistently observed phenomenon is beyond the scope of the present paper but could be a subject of future work.

VI. DISCUSSION AND CONCLUSION

We have observed Rydberg EIT in a vapor cell containing 5 Torr of Ne buffer gas. Results obtained at low probe power have revealed frequency shifts of the EIT signals by about 70 MHz, as well as an increased FWHM EIT linewidth of about 120 MHz. These observations are largely unaffected by variations in the principal quantum number of the Rydberg states and in the probe power, as long as the probe Rabi frequency remains below about 10 MHz. The frequency shift is attributed to low-energy *s*-wave scattering between the Rydberg electron and the Ne atoms and polarization of the Ne atoms by the atomic electric field. The width of the signal is dominated by polarization of the Ne atoms. At high probe power, we observe a transition from EIT to EIA; this phenomenon awaits a future explanation. In electric-field-sensing applications, discussed next, it is suggested that probe powers are used that are sufficiently low to avoid complications of the data analysis caused by the EIT to EIA transition.

Utilizing the Stark effect of Rydberg levels, potential applications of our research include noninvasive and spatially resolved measurement of electric fields in low-pressure discharge plasmas. As fields of use we envision dc, rf, dusty, and afterglow plasmas in the sub-500-mTorr regime. There, buffer-gas-induced shifts and linewidths will be reduced by a factor of 10 or more relative to those in our present 5-Torr data, because shifts and widths are proportional to density [see Eqs. (1)–(3)]. In the sub-500-mTorr regime, shifts and widths will be on the order of the EIT linewidth, and will typically be outweighed by the Stark shifts of interest. We do not expect the Rydberg-EIT method to be competitive for high-pressure discharge and high-density laser plasma with pressures above about 5 Torr, due to EIT signal degradation at higher pressures.

Specifically, the electric fields of highly charged dust particles in low-density plasma could be spatially mapped using Rydberg EIT. Since in the sub-500-mTorr regime the EIT lines will be about 10 times narrower and considerably taller than in our present work, systematic effects, such as line pulling by unresolved levels and laser-power changes during the scans, are expected to become irrelevant. Also, pressure shifts will be about 10 times less than those in Fig. 2(a) and tend to become insignificant. We believe that Rydberg EIT will be well-suited for spatio-temporal mapping of electric fields in low-pressure discharge plasma and near highly charged dust particles in such plasma.

Aside from plasma electric field sensing, for pressures up to about 5 Torr we see applications of Rydberg EIT as a real-time, in-situ, and noninvasive readout for buffer-gas density. The Rydberg-EIT probe can be applied at an exact location of interest, which can have advantages over reading the buffer-gas pressure at a remote pressure gauge. In view of the density scaling in Eqs. (1)–(3), we believe that at pressures much larger than about 5 Torr the Rydberg-EIT lines will become too shallow and too wide to still be observable with the method explored in this paper.

ACKNOWLEDGMENTS

We acknowledge fruitful discussions with Professor Eric Paradis (Eastern Michigan University), Dr. David A. Anderson (Rydberg Technologies Inc.), and Bineet Dash (University of Michigan). This project was supported by the U.S. Department of Energy, Office of Science, Office of Fusion Energy Sciences under award number DE-SC0023090. N.T. acknowledges funding from the NSRF via the Program Management Unit for Human Resources and Institutional Development, Research and Innovation (Grant No. B37G660011), and from the Office of the Permanent Secretary, Ministry of Higher Education, Science, Research and Innovation (Grant No. RGNS.64-067). R.C. acknowledges support from a Rackham Predoctoral Fellowship of the University of Michigan.

[1] J. A. Sedlacek, A. Schwettmann, H. Kübler, R. Löw, T. Pfau, and J. P. Shaffer, Microwave electrometry with Rydberg atoms in a vapour cell using bright atomic resonances, Nat. Phys. **8**, 819 (2012).

[2] J. A. Sedlacek, A. Schwettmann, H. Kübler, and J. P. Shaffer, Atom-based vector microwave electrometry using rubidium Rydberg atoms in a vapor cell, Phys. Rev. Lett. **111**, 063001 (2013).

[3] C. L. Holloway, J. A. Gordon, S. Jefferts, A. Schwarzkopf, D. A. Anderson, S. A. Miller, N. Thaicharoen, and G. Raithel, Broadband Rydberg atom-based electric-field probe for si-traceable, self-calibrated measurements, IEEE Trans. Antennas Propag. **62**, 6169 (2014).

[4] D. A. Anderson, R. E. Sapiro, and G. Raithel, Rydberg atoms for radio-frequency communications and sensing: Atomic receivers for pulsed rf field and phase detection, IEEE Aerosp. Electron. Syst. Mag. **35**, 48 (2020).

[5] David H. Meyer, Paul D. Kunz, and Kevin C. Cox, Waveguide-coupled Rydberg spectrum analyzer from 0 to 20 GHz, Phys. Rev. Appl. **15**, 014053 (2021).

[6] David Alexander Anderson, Rachel Elizabeth Sapiro, and Georg Raithel, An atomic receiver for AM and FM radio communication, IEEE Trans. Antennas Propag. **69**, 2455 (2021).

[7] D. Feldbaum, N. V. Morrow, S. K. Dutta, and G. Raithel, Coulomb expansion of laser-excited ion plasmas, Phys. Rev. Lett. **89**, 173004 (2002).

[8] Alisher Duspayev and Georg Raithel, Electric field analysis in a cold-ion source using Stark spectroscopy of Rydberg atoms, Phys. Rev. Appl. **19**, 044051 (2023).

[9] David A. Anderson, Georg Raithel, Matthew Simons, and Christopher L. Holloway, Quantum-optical spectroscopy for plasma electric field measurements and diagnostics, arXiv:1712.08717.

[10] Daniel Weller, James P. Shaffer, Tilman Pfau, Robert Löw, and Harald Kübler, Interplay between thermal Rydberg gases and plasmas, Phys. Rev. A **99**, 043418 (2019).

[11] Lu Ma, Eric Paradis, and Georg Raithel, Dc electric fields in electrode-free glass vapor cell by photoillumination, Opt. Express **28**, 3676 (2020).

[12] Armen Sargsyan, David Sarkisyan, Ulrich Krohn, James Keaveney, and Charles Adams, Effect of buffer gas on an electromagnetically induced transparency in a ladder system using thermal rubidium vapor, Phys. Rev. A **82**, 045806 (2010).

[13] Wan-Ü. L. Brillet and A. Gallagher, Inert-gas collisional broadening and shifts of Rb Rydberg states, Phys. Rev. A **22**, 1012 (1980).

[14] K. H. Weber and K. Niemax, Impact broadening and shift of Rb *nS* and *nD* levels by noble gases, Zeitschrift für Physik A Atoms and Nuclei **307**, 13 (1982).

[15] D. M. Bruce, M. Y. Mirza, and W. W. Duley, Collision broadening and shift of the S and D Rydberg levels of rubidium by He and Ar, Opt. Commun. **40**, 347 (1982).

[16] D. C. Thompson, E. Kammermayer, B. P. Stoicheff, and E. Weinberger, Pressure shifts and broadenings of Rb Rydberg states by Ne, Kr, and H_2, Phys. Rev. A **36**, 2134 (1987).

[17] William E. Bell, Arnold L. Bloom, and James Lynch, Alkali metal vapor spectral lamps, Rev. Sci. Instrum. **32**, 688 (1961).

[18] Richard G. Brewer, High intensity low noise rubidium light source, Rev. Sci. Instrum. **32**, 1356 (1961).

[19] P. K. Shukla and B. Eliasson, Colloquium: Fundamentals of dust-plasma interactions, Rev. Mod. Phys. **81**, 25 (2009).

[20] C. J. Mitchell, M. Horányi, O. Havnes, and C. C. Porco, Saturn's spokes: Lost and found, Science **311**, 1587 (2006).

[21] Nilton O. Renno, Ah-San Wong, Sushil K. Atreya, Imke de Pater, and Maarten Roos-Serote, Electrical discharges and broadband radio emission by Martian dust devils and dust storms, Geophys. Res. Lett. **30**, 2140 (2003).

[22] S. I. Popel, L. M. Zelenyi, A. P. Golub', and A. Yu. Dubinskii, Lunar dust and dusty plasmas: Recent developments, advances, and unsolved problems, Planet. Space Sci. **156**, 71 (2018).

[23] S. Ratynskaia, A. Bortolon, and S. I. Krasheninnikov, Dust and powder in fusion plasmas: Recent developments in theory, modeling, and experiments, Rev. Mod. Plasma Phys. **6**, 20 (2022).

[24] Laïfa Boufendi, M Jouanny, Eva Kovacevic, Johannes Berndt, and Maxime Mikikian, Dusty plasma for nanotechnology, J. Phys. D: Appl. Phys. **44**, 174035 (2011).

[25] Robert L. Merlino, Dust-acoustic waves driven by an ion-dust streaming instability in laboratory discharge dusty plasma experiments, Phys. Plasmas **16**, 124501 (2009).

[26] Mohamad Menati, Edward Thomas, and Mark J. Kushner, Filamentation of capacitively coupled plasmas in large magnetic fields, Phys. Plasmas **26**, 063515 (2019).

[27] Markus H. Thoma, Hubertus M. Thomas, Christina A. Knapek, Andre Melzer, and Uwe Konopka, Complex plasma research under microgravity conditions, npj Microgravity **9**, 13 (2023).

[28] T. E. Sheridan, N. R. Weiner, and T. E. Steinberger, Dust and plasma properties measured using two confined particles, J. Plasma Phys. **82**, 615820304 (10 pp.) (2016).

[29] E. Joshi, M. Y. Pustylnik, M. H. Thoma, H. M. Thomas, and M. Schwabe, Recrystallization in string-fluid complex plasmas, Phys. Rev. Res. **5**, L012030 (6 pp.) (2023).

[30] D. Budker, W. Gawlik, D. F. Kimball, S. M. Rochester, V. V. Yashchuk, and A. Weis, Resonant nonlinear magneto-optical effects in atoms, Rev. Mod. Phys. **74**, 1153 (2002).

[31] J. C. Allred, R. N. Lyman, T. W. Kornack, and M. V. Romalis, High-sensitivity atomic magnetometer unaffected by spin-exchange relaxation, Phys. Rev. Lett. **89**, 130801 (2002).

[32] V. A. Alekseev and I. I. Sobel'man, A spectroscopic method for the investigation of elastic scattering of slow electrons, Sov. Phys. JETP **22**, 882 (1966).

[33] A. Omont, On the theory of collisions of atoms in Rydberg states with neutral particles, J. Phys. France **38**, 1343 (1977).

[34] U. Asaf, K. Rupnik, G. Reisfeld, and S. P. McGlynn, Pressure shifts and electron scattering lengths in atomic and molecular gases, J. Chem. Phys. **99**, 2560 (1993).

[35] Enrico Fermi, Sopra lo spostamento per pressione delle righe elevate delle serie spettrali, Il Nuovo Cimento (1924–1942) **11**, 157 (1934).

[36] Ch Ottinger, Richard Scheps, G. W. York, and Alan Gallagher, Broadening of the Rb resonance lines by the noble gases, Phys. Rev. A **11**, 1815 (1975).

[37] Till Ockenfels, Paško Roje, Thilo vom Hövel, Frank Vewinger, and Martin Weitz, Spectroscopy of high-pressure rubidium–noble-gas mixtures, Phys. Rev. A **106**, 012815 (2022).

[38] A. Sargsyan, T. A. Vartanyan, and D. Sarkisyan, Broadening and shift of the D_1 and D_2 lines of Rb atoms by neon: Resolving hyperfine components in a half-wave cell using double differentiation with respect to frequency, Opt. Spectrosc. **129**, 1173 (2021).

[39] Wenhui Li, I. Mourachko, M. W. Noel, and T. F. Gallagher, Millimeter-wave spectroscopy of cold Rb Rydberg atoms in a magneto-optical trap: Quantum defects of the *ns*, *np*, and *nd* series, Phys. Rev. A **67**, 052502 (2003).

[40] L. Ma, D. A. Anderson, and G. Raithel, Paschen-back effects and Rydberg-state diamagnetism in vapor-cell electromagnetically induced transparency, Phys. Rev. A **95**, 061804 (2017).

[41] Megan E. Henry and Roger M. Herman, Collisional broadening of Rydberg atom transitions by rare gas perturbers, J. Phys. B **35**, 373 (2002).

[42] C. R. Hoffmann and H. M. Skarsgard, Momentum-transfer cross sections and conductivity ratios for low-energy electrons in He, Ne, Kr, and Xe, Phys. Rev. **178**, 168 (1969).

[43] Kamil Fedus, Electron scattering from neon via effective range theory, Braz. J. Phys. **44**, 622 (2014).

[44] Yongjun Cheng, Li Yan Tang, J. Mitroy, and M. S. Safronova, All-order relativistic many-body theory of low-energy electron-atom scattering, Phys. Rev. A **89**, 012701 (2014).

[45] Daniel A. Steck, Rubidium 85 d line data (2023), https://steck.us/alkalidata/.